nature portfolio
https://doi.org/10.1038/s41596-021-00532-2

Supplementary information

Surgical implantation of wireless, battery-free optoelectronic epidural implants for optogenetic manipulation of spinal cord circuits in mice

In the format provided by the authors and unedited

Supplemental Information:

Supplementary Methods:

Design and functionality of the spinal optoelectronic device – The double loop wire antenna (operating at 13.56 MHz) provides a uniform magnetic field inside the cage as shown by the vector and contour plots obtained from FEA simulations (Figure S2). Increasing the power in the antenna (1-12 W) increases the magnetic field strength but the field distribution in the XY (Figure S3b) and YZ (Figure S3c) planes remain relatively uniform even at high powers, except in the regions close to the copper wire where the magnetic field strength is higher (Y = ± 16 cm in Figure S3c). For fixed values of X and Y (e.g., mouse located at the center of the cage) the magnetic field results in Figure S3B show the strongest magnetic field ~5 cm (approximate height location of implanted receiver coil) from the bottom of the cage. Figure S3d shows the results when the mouse moves laterally to another location in the cage (Y = ± 12.5 cm), the magnetic field strength increases due to its proximity with the copper wire. Further, for a fixed value of Z (i.e., implant receiver remains at the same height), the magnetic field results in Figure S3e show a uniform field even when the mouse moves laterally (in Y coordinate) inside the cage. For the antenna working at 13.56 MHz with a power input of 9.25 W, the magnetic field strength inside the cage is ~ 4.5 A/m except in the regions close to the copper wires where the magnetic field can reach ~ 8.1 A/m.

The commercial software ANSYS HFSS was used to perform electromagnetic finite element analysis and determine the magnetic field distribution inside a 10 x 33 x 10 cm3 cage (length x width x height) enclosed by a copper wire antenna (diameter = 22 AWG) with two loops. The bottom and top loops are placed at 3 cm and 6 cm, respectively, above the cage floor to create a uniform magnetic field. A lumped port was used to obtain the port impedance Z of the wire antenna and tune it to a working frequency of 13.56 MHz. An adaptive mesh (tetrahedron elements) and a spherical radiation boundary (radius of 2500 mm) were adopted to ensure computational accuracy. The bulk conductivity, relative permittivity, and relative permeability of copper wire are σCu = 5.8 x 107 S/m, εCu = 1, and μCu = 0.99, respectively.

A lumped port was used to obtain the scattering parameter S11 for the double layer copper receiver coil with a 56-pF external capacitor. The inductance (L) and Q factor (Q) at 13.56 MHz were obtained as L = Im{Znn}/(2π f) = 2.5 μH. and Q = |Im{Znn}/Re{Znn}| = 22, where Re{Znn}, Im{Znn}, and f represent the real and imaginary parts of Z, and the working frequency.

Lastly, the specific absorption rate (SAR), a measure of radio frequency energy absorption in the mouse body, was calculated, with a receiver coil in a plastic cage with a double loop copper wire transmission antenna operating at 13.56 MHz shown in Figure S4a. A simplified mouse mesh ellipsoid body with major (half) axes 5, 8.5, and 32.5 mm shown in Figure S4b shows that the SAR is well below the safety guidelines of radio frequency exposure[1]. The bulk conductivity, relative permittivity, and relative permeability of the mouse mesh body are σMouse = 0.27 S/m, εMouse = 2000, and μMouse = 0.99, respectively. We performed simulation to measure the SAR level at 13.56 MHz, at which the RF reader operates. The results (0.02 W/kg) show SAR level far below the limits for commercial equipment (1-2 W/kg). For the mouse located at the center of the cage (Figure S4a), the maximum SAR from FEA results is 0.02 W/kg (Figure S4b), well below the safety guidelines of radio frequency exposure[1].

Figure S5 shows the temperature distributions of the implanted probe. The YZ and XY plane temperature profiles allow us to compute the temperature change as a function of distance from the μLED through the spinal cord. For a stimulation frequency of 5Hz and a pulse duration of 5 ms, the maximum ΔT is ~ 0.17 ^{o}C directly above the μLED and it decays through the spinal cord as the distance away from the μLED increases. Changing the pulse duration to 2 ms and 1 ms will result in maximum ΔT is ~ 0.07 ^{o}C and ~ 0.03 ^{o}C at the surface of the probe (Figure S5), respectively. The ΔT as a function of time is given in Figure S5c for different stimulation frequencies but a fixed pulse duration (5 ms). Figure S5d presents a parametric study to understand the influence of the pulse duration (ms) and stimulation frequency (Hz) on the maximum ΔT and select both parameters accordingly to minimize the ΔT. In Figure S5c and S5d, the temperature change was averaged over the probe surface area of 0.42 mm^2 directly below the μLED.

Transient heat transfer analysis was implemented with the commercial software ABAQUS (Analysis User's Manual 2010, V6.10) to compute the temperature change (ΔT) in the spinal cord and surrounding tissues due to the thermal power of µLED for stimulation frequencies of 1-5 Hz and pulse duration 1-5 ms. Heat generated from metabolism and blood perfusion effects are not considered in the analysis. The Pennes' bio-heat equation is given by: $\rho C_p \frac{\partial T}{\partial t} + \nabla \cdot (-k \nabla T) = Q_{the}$; where T is temperature, t is time; k, ρ, and C_p are the thermal conductivity, mass density and heat capacity of the spinal cord and tissues. Q_{the} is the heat generated by thermal power of µLEDs ~15 mW [2]. The spinal cord and tissues, probe geometry, and the µ-LEDs were modeled using a 10-node quadratic heat transfer tetrahedron (DC3D10). Convergence tests of the mesh size were performed to ensure accuracy. The total number of elements in the models was approximately 560,000. The thermal conductivity, specific heat capacity, and density of the materials/tissues used in the simulation are $k_{Cu} = 377$ W·m^{-1}·K^{-1} , $C_{p_{Cu}} = 385$ J·kg^{-1}·K^{-1}, and $\rho_{Cu} = 8960$ kg·m^{-3} for copper; $k_{PI} = 0.21$ W·m^{-1}·K^{-1} , $C_{p_{PI}} = 2100$ J·kg^{-1}·K^{-1}, and $\rho_{PI} = 909$ kg·m^{-3} for polyimide (PI); $k_{\mu LED} = 130$ W·m^{-1}·K^{-1} , $C_{p_{\mu LED}} = 490$ J·kg^{-1}·K^{-1}, and $\rho_{\mu LED} = 6100$ kg·m^{-3} for the µLED; $k_{Skin} = 0.322$ W·m^{-1}·K^{-1} , $C_{p_{Skin}} = 3350$ J·kg^{-1}·K^{-1}, and $\rho_{Skin} = 1090$ kg·m^{-3} for the skin layer; $k_{Fat} = 0.21$ W·m^{-1}·K^{-1} , $C_{p_{Fat}} = 3660$ J·kg^{-1}·K^{-1}, and $\rho_{Fat} = 911$ kg·m^{-3} for the subcutaneous fat layer; $k_{Bone} = 0.45$ W·m^{-1}·K^{-1} , $C_{p_{Bone}} = 1313$ J·kg^{-1}·K^{-1}, and $\rho_{Bone} = 1908$ kg·m^{-3} for the vertebral bone; $k_{spinal\ cord} = 0.51$ W·m^{-1}·K^{-1} , $C_{p_{spinal\ cord}} = 3630$ J·kg^{-1}·K^{-1}, and $\rho_{spinal\ cord} = 1075$ kg·m^{-3} for the spinal cord.

In addition to running thermal simulation as described above, we also measured the temperature of the uLED *in* vitro while submerged in saline solution to replicate the condition *in vivo* under varying stimulation parameters (Figure S6). The measurements yield an almost-zero temperature increase (±0.1 ˚C) on the µLED when the device is placed on the corner of the enclosure at the highest harvested power.

References

1. Bailey, W. H. *et al.* Synopsis of IEEE Std C95.1™-2019 'IEEE Standard for Safety Levels with Respect to Human Exposure to Electric, Magnetic, and Electromagnetic Fields, 0 Hz to 300 GHz'. *IEEE Access* **7**, 171346–171356 (2019).
2. Stujenske, J. M., Spellman, T. & Gordon, J. A. Modeling the Spatiotemporal Dynamics of Light and Heat Propagation for InVivo Optogenetics. *Cell Rep.* **12**, 525–534 (2015).

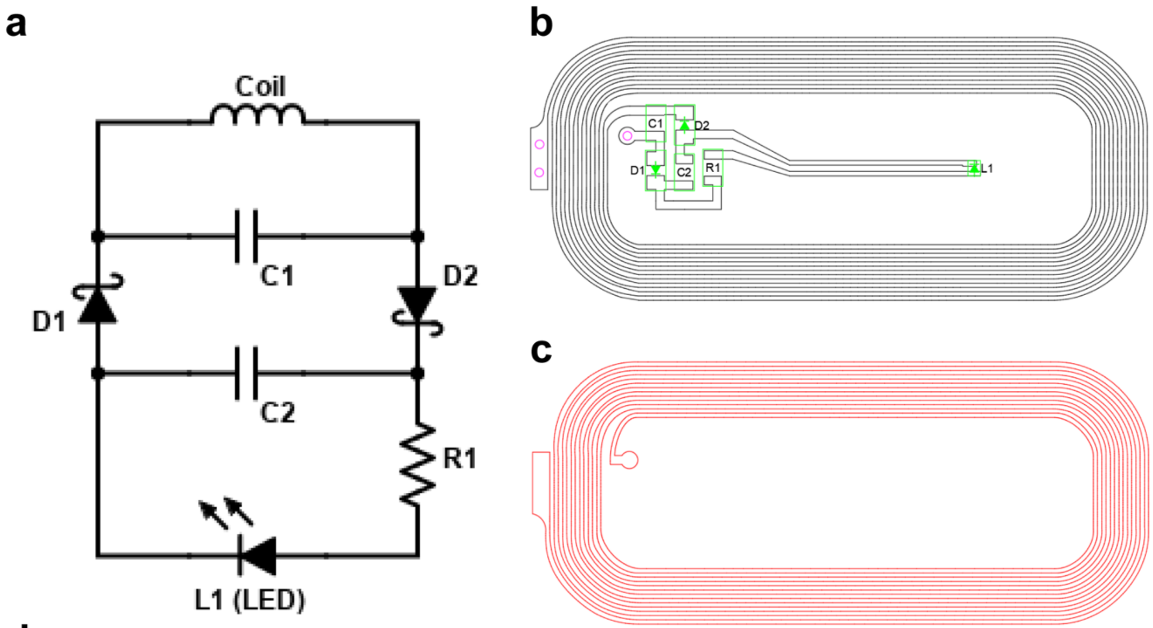

d

	Description	Part #	Manufacturer
C1	Capacitor, 56 pF, 0.6 mm x 0.3 mm x 0.3 mm	250R05L560JV4T	Johanson Technology Inc
D1, D2	Schottky diode, 0.62 mm x 0.32 mm x 0.32 mm	CDBZ0130R-HF	Comchip Technology
R1	Resistor, 0 ohm, 0.6 mm x 0.3 mm x 0.23 mm	CRCW020110R0FNED	Vishay Dale
C2	Capacitor, 2.2 uF, 0.6mm x 0.3mm x 0.3mm	GRM033R61A225KE47D	Murata Electronics
L1	Simulating LED, 465nm, 220 µm x 270 µm x 50 µm	C460TR2227-0216	Cree Inc

Supplemental Figure 1. µLED device electronic components. (**a**) Circuit diagram. (**b**) Front side of the PCB with the assembly map. (**c**) Back side of the device. (**d**) List of circuit components.

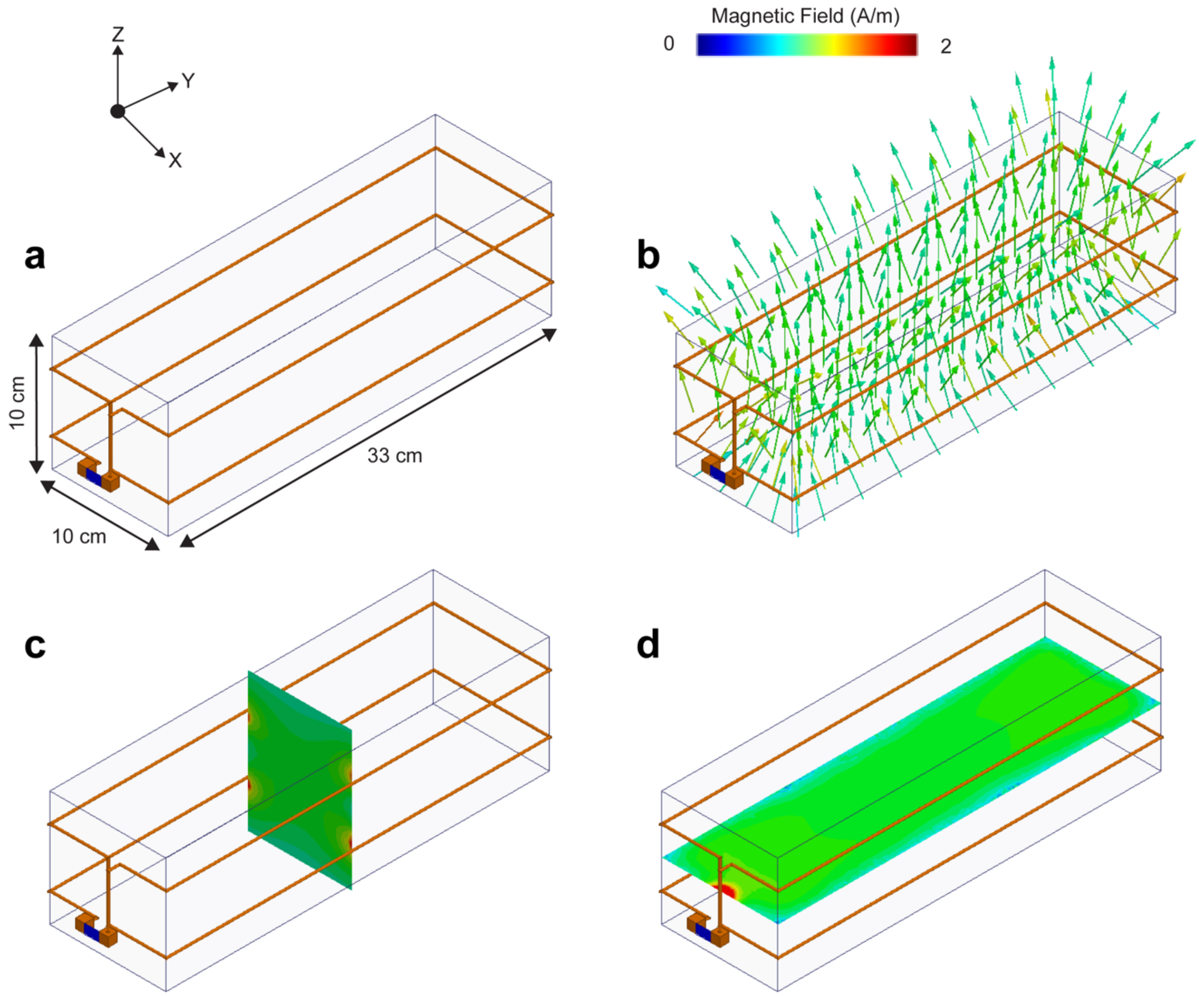

Supplemental Figure 2. Cage schematics and electromagnetic performance. (**a**) Double loop antenna wiring layout (diameter = 22 AWG) in the cage with dimensions 10 cm x 33 cm x 10 cm (W x L x H). (**b**) Simulated magnetic vector field distribution inside the cage. The uniform magnetic field (A/m) inside the cage distribution is shown at the (**c**) ZX plane (Y=0 cm) and. (**d**) in YX plane (Z=5 cm) for an input power of 1W.

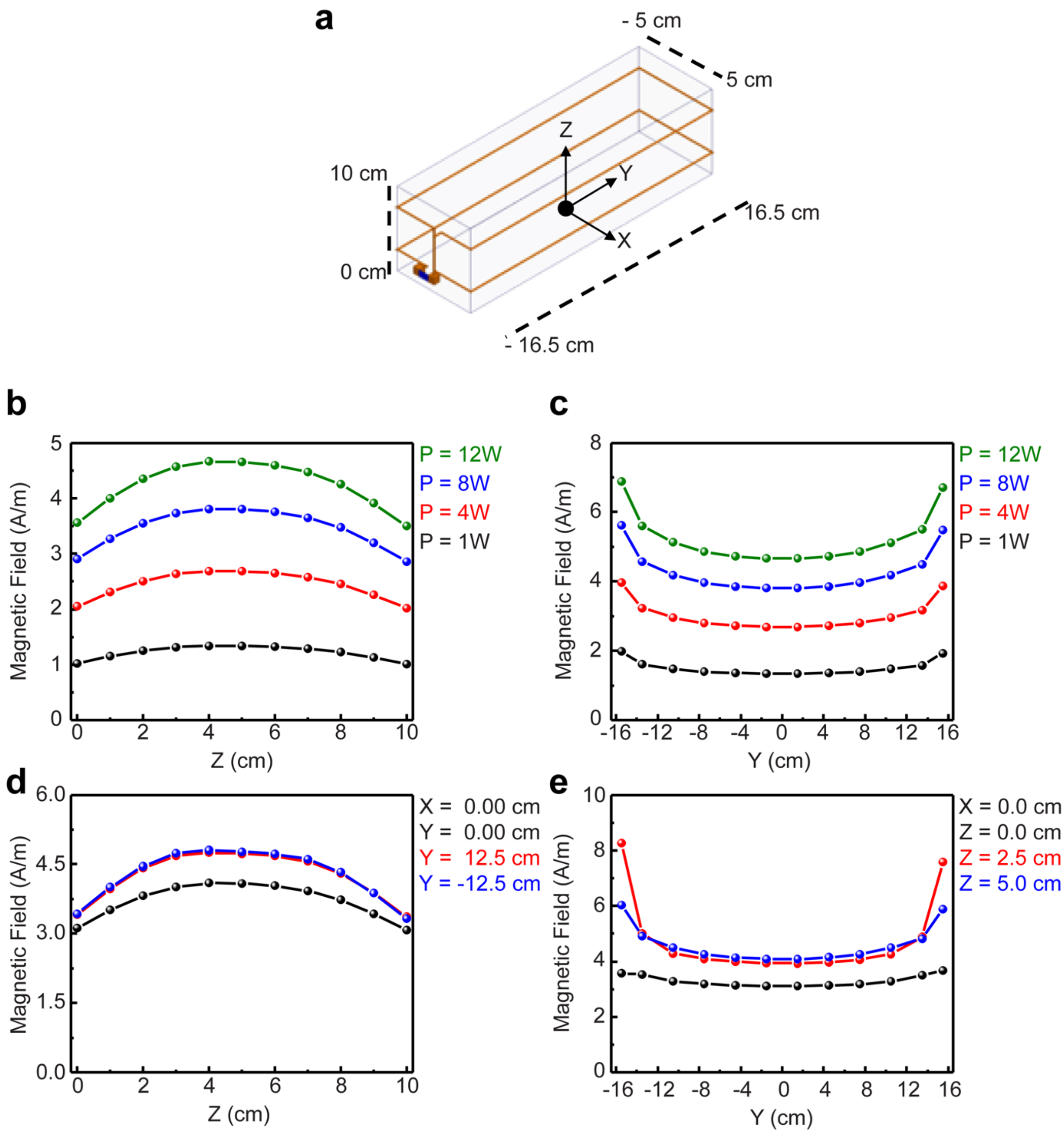

Supplemental Figure 3. Influence of input power and location inside the cage magnetic field. (**a**) Coordinate system (X, Y, Z) inside the cage; the point (0, 0, 0) cm is located at the center of the cage floor. Simulated magnetic field strength (A/m) for input power ranging from 1- 12 W at the locations (**b**) (0, 0, Z) cm and (**c**) (0, Y, 5) cm to show magnetic field uniformity vertically and laterally, respectively. For a fixed power 9.25 W used in experiments, the simulated magnetic field strength at (**d**) (0, [0,±12.5], Z) cm shows the uniformity of the field vertically through the cage when the mouse moves to a different Y location inside the cage and at (**e**) (0,Y, [0, 2.5 5]) cm captures the magnetic field strength horizontally at different Z locations of the implant.

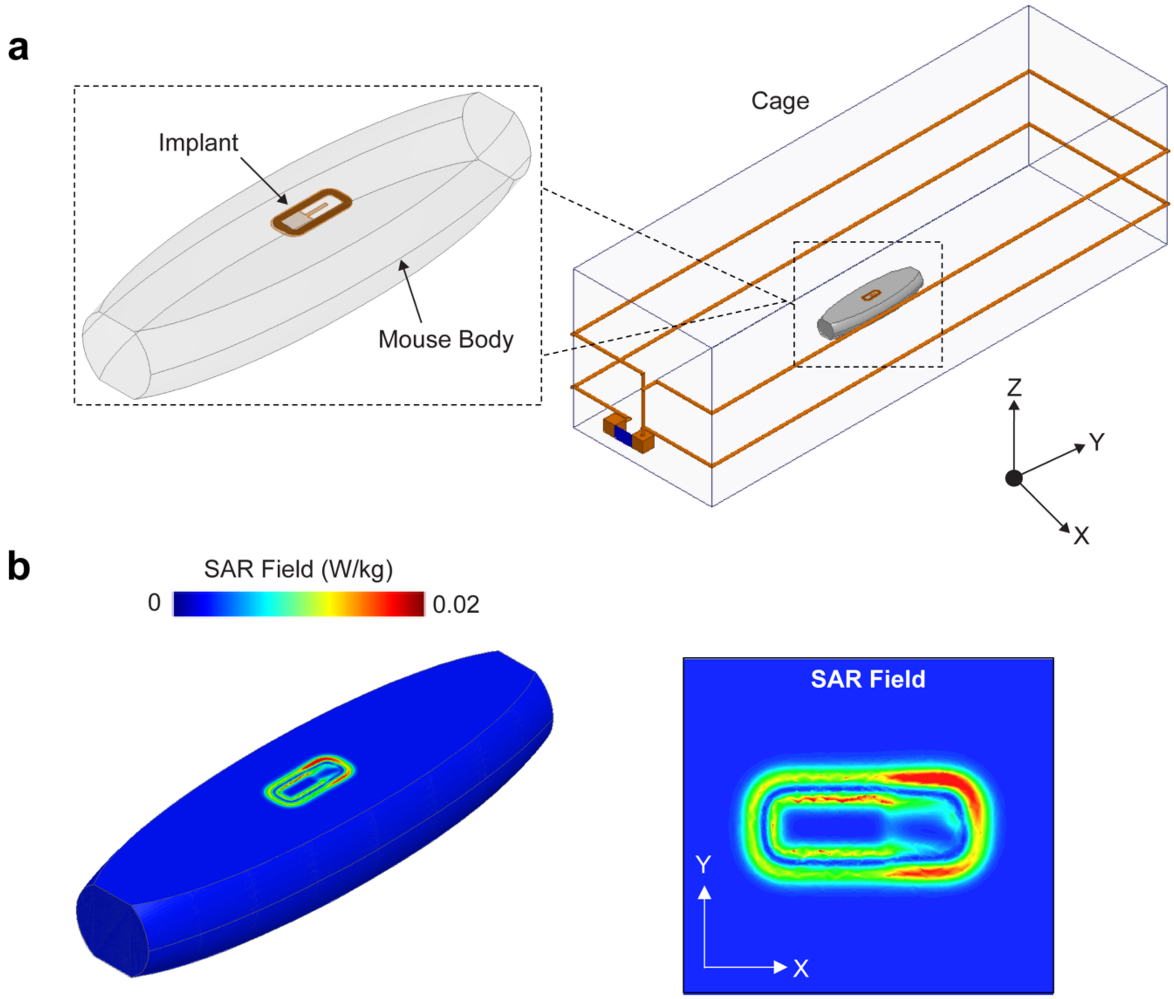

Supplemental Figure 4. Electromagnetic energy absorbed by the mouse body. (**a**) Simplified mouse ellipsoid body with implant receiver coil inside the cage operating at 13.56 MHz with input power 9.25 W. (**b**) Simulated average Specific Absorption Rate (SAR) field contour in the 3D mouse ellipsoid body and in the XY plane above the implant, where the highest value (0.02 W/kg) falls well below the recommended safety exposure.

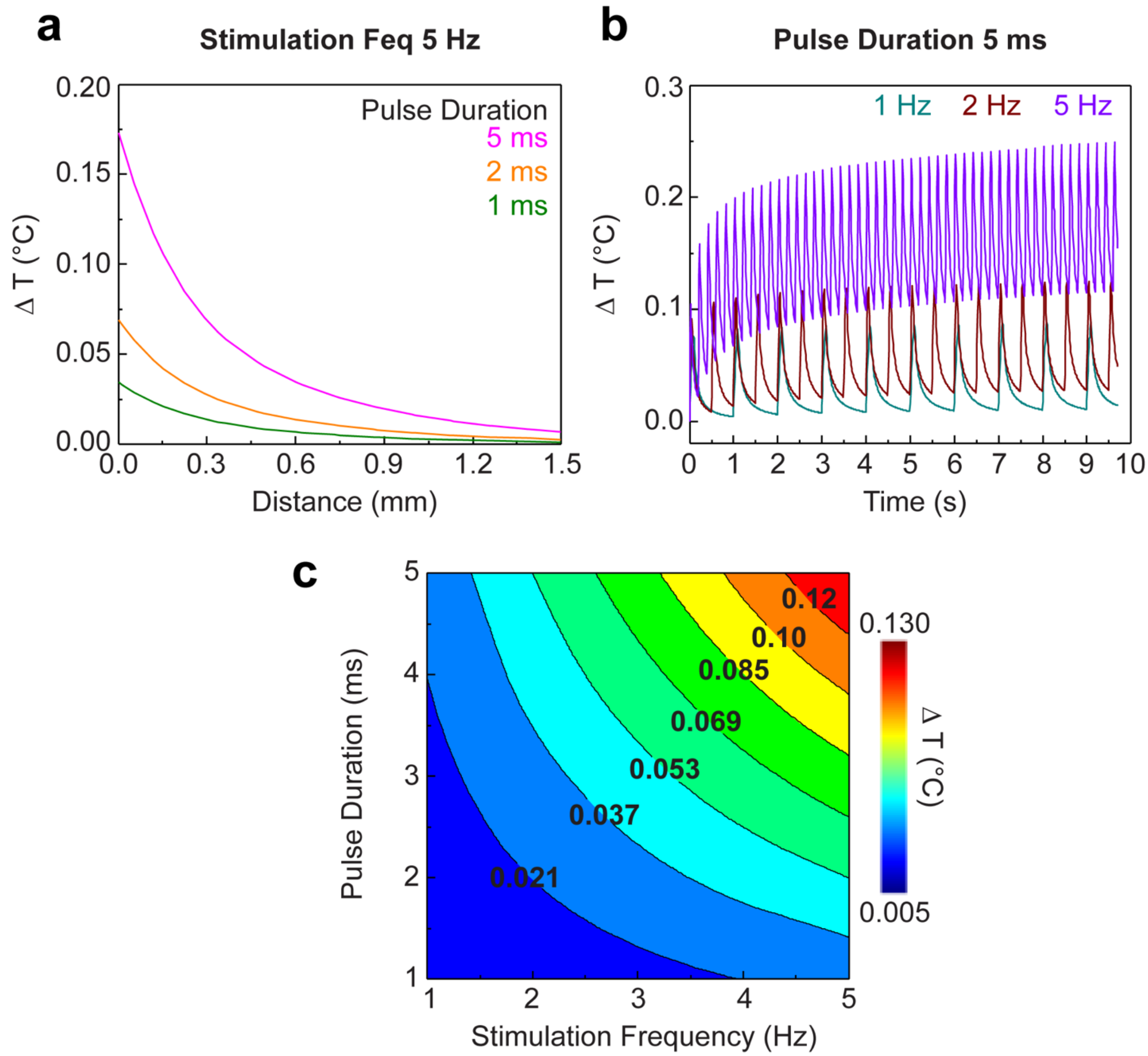

Supplemental Figure 5. Effect of μLED stimulation parameters on the temperature change. (**a**) Simulated temperature change (degrees Celsius) for 1 ms, 2 ms, and 5 ms pulse duration as a function of distance away from the μLED at a fixed stimulation frequency of 5Hz. (**b**) Time history of the simulated temperature change (degrees Celsius) averaged over the surface area directly above the μLED for 1 Hz, 2 Hz, and 5 Hz stimulation frequency with a fixed pulse duration of 5 ms. (**c**) Parametric study of temperature change in the surface area directly above the μLED for variable stimulation frequency (Hz) and pulse duration (ms).

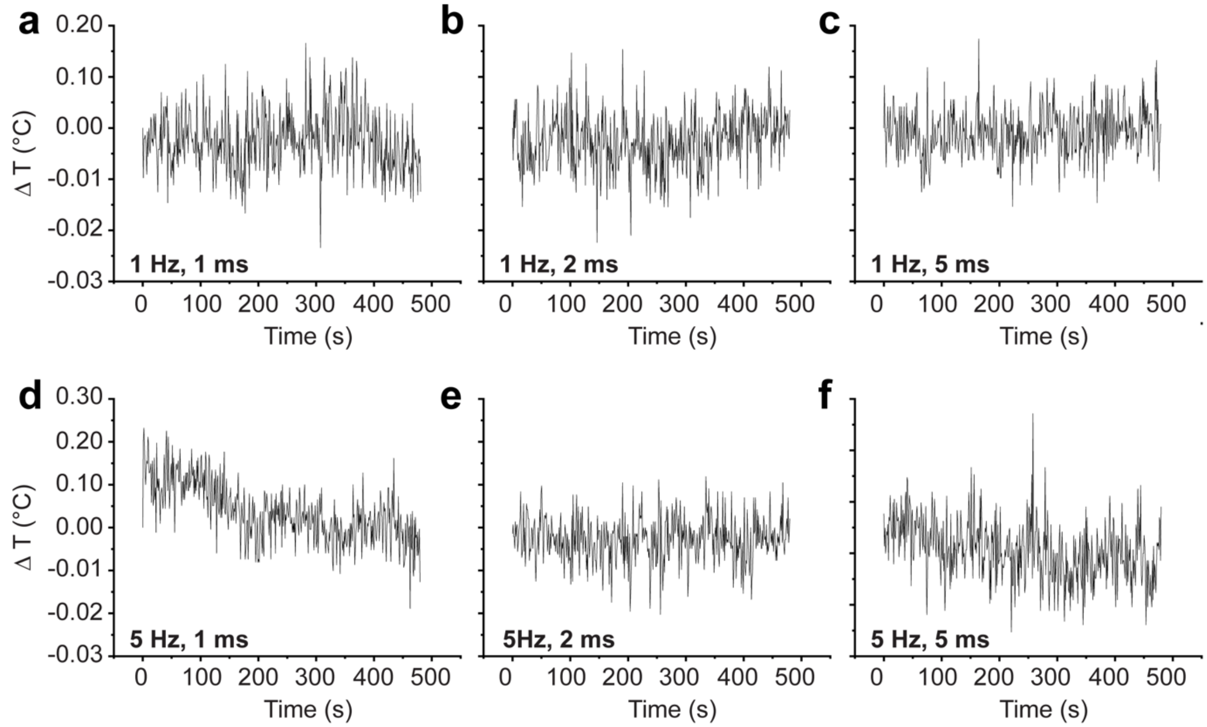

Supplemental Figure 6. IR temperature measurement of the µLED. Using an IR camera, the temperature of the µLED from a device on the corner of a 30 cm x 10 cm x 10 cm (LxWxH) enclosure (where the power harvested is the highest). (**a-c**) Using a 1 Hz frequency, we varied the width (ms) of the µLED pulse to 1ms, 2ms and 5ms respectively. (**d-f**) Using a 5 Hz frequency, we varied the width (ms) of the µLED pulse to 1ms, 2ms and 5ms respectively.